COMMUNICATION

Check for updates

Analysis of hydrogen in a hydrogenated, 3D-printed Ti–6Al–4V alloy by glow discharge optical emission spectroscopy: sample heating effects

Zdeněk Weiss, [ID] *[a] Jaroslav Čapek,[a] Zdeněk Kačenka,[ab] Ondřej Ekrt,[a] Jaromír Kopeček, [ID] [a] Monika Losertová [ID] [c] and Dalibor Vojtěch[b]

Depth profile analysis of a hydrogenated Ti–6Al–4V alloy by glow discharge optical emission spectroscopy (GDOES) is described. Besides the earlier reported 'hydrogen effects', causing changes in emission intensities of other elements if hydrogen is present, the analysis of hydrogen itself was found to be affected by the redistribution of hydrogen in the region adjacent to the analyzed spot, due to sample heating and the thereby increased hydrogen diffusivity. A simple model of heat transfer within the sample during the GDOES analysis is proposed and the surface temperature of the analyzed spot is estimated to be ≈365 °C, in the given experimental setup.

1. Introduction

Ti–6Al–4V is one of the most common alpha–beta titanium alloys, widely used in a large number of technical and biomedical applications.[1,2] The mechanical properties of titanium-based and other engineering alloys can be adversely affected by hydrogen. However, temporary hydrogen alloying by a special heat treatment technology, the so-called thermohydrogen treatment (THT),[3,4] allows hot workability of α + β titanium alloys at lower temperatures with lower flow stresses, to improve the fatigue and strength properties. The interactions of hydrogen with titanium-based materials, mainly with Ti–6Al–4V, have been of interest in the context of hydrogen embrittlement or when considering these materials as potential candidates for hydrogen storage.[5,6] In these applications, a demand has arisen to analyze hydrogen in hydrogenated Ti–6Al–4V, for the total hydrogen content in a bulk material and a depth-

resolved analysis of the elements present in the near-surface region. Analysis of hydrogen in inorganic materials is in many respects special, compared to the analysis of other elements, and the portfolio of methods available for this purpose is rather limited.[7] The purpose of this note is to summarize the results obtained in this application using Glow Discharge Optical Emission Spectroscopy (GDOES), to describe the methodology used and analytical interpretation of the experimental data.

GDOES is a relatively well accessible method, capable of analyzing hydrogen. In the conventional analysis by GDOES of metals and alloys, a robust, accurate and self-consistent calibration/quantification scheme exists.[8] The central relation linking glow discharge emission intensities of analytical lines, $I_{E,M}$, and the concentrations $c_{E,M}$ of the respective elements, analyzed in a matrix (sample) M, is as follows:

$$I_{E,M} = R_E c_{E,M} q_M \qquad (1)$$

where q_M is the sputtering rate of the sample (the matrix) M. The proportionality constant R_E, called the emission yield, is considered independent of the matrix analyzed. This allows for quantitative multi-matrix analyses with sputter rate-corrected calibrations, based on bulk reference materials with known composition and known sputtering rates. This approximation, however, breaks down in the presence of hydrogen,[9–11] and further corrections are necessary to interpret raw data resulting from the analysis correctly. Possible mechanisms and various correction schemes of those 'hydrogen effects' have been the subject of considerable attention by various groups, as well as efforts to develop suitable reference materials for hydrogen analysis by GDOES.[12,13] Besides the emission intensities of the analysed elements being affected by hydrogen, an even more peculiar behaviour was observed in the present work, in the analysis of 3D-printed hydrogenated Ti–6Al–4V samples by GDOES, and attributed to the relocation of hydrogen within the sample during the analysis, followed by its entering the plasma. This and a proposed explanation of such phenomena is the topic of this note.

[a]FZU – Institute of Physics of the Czech Academy of Sciences, Na Slovance 2, 182 00, Praha 8, Czech Republic. E-mail: weissz@fzu.cz

[b]University of Chemistry and Technology, Faculty of Chemical Technology, Department of Metals and Corrosion Engineering, Technická 5, Dejvice, 166 28, Praha 6, Czech Republic

[c]Department of Materials Engineering and Recycling, Faculty of Materials Science and Technology, VSB – Technical University of Ostrava, 17. listopadu 2172/15, Poruba, 708 00, Ostrava, Czech Republic

2. Experimental

The Ti–6Al–4V samples were prepared by selective laser melting (SLM). In this process, a fine (several tens of μm) Ti–6Al–4V powder is evenly distributed onto a metallic platform and subsequently fused by melting with a high-power laser beam, scanned over a 2D cross-section of the desired shape. The powder spreading and laser melting steps are then alternately repeated until the complete 3D shape of the manufactured part is achieved. The CL 41 TI ELI powder (ConceptLaser, particle mean size of 45 μm) was used as the initial powder. The SLM process was performed using the M2 Cusing machine (ConceptLaser) at the following conditions: laser power of 200 W, scanning speed of 0.8 m s^{-1}, chessboard scanning strategy with boxes of 5 × 5 mm^2, hatch distance of 120 μm. The samples were printed in vertical orientation. The prepared samples were of the flat dog-bone shape with a thickness of 3 mm. The width and the length of the working part were 5 and 25 mm respectively. The anchor parts of the tensile samples were 15 mm in length, 7.5 mm in width and 3 mm in thickness. At the end, the as-printed samples were surface finished by milling. The final roughness of the samples was 1.6 μm. Those samples were subsequently hydrogenated in a Linn HT1800 furnace at 800 °C (reached at a heating rate of 1000 °C h^{-1}) for 1 hour and at a low overpressure of 700 Pa. The purity of the hydrogen gas was 6 N. After the hydrogenation, a two-step cooling was performed: in flowing hydrogen to the temperature of 200 °C and then in flowing argon of 5 N purity to 120 °C. Thereafter the specimens were removed from the furnace.

GDOES analyses were made using the GDA750HR spectrometer (Spectruma GmbH., Germany), with a DC discharge in argon and a 2.5 mm-internal anode diameter Grimm-type spectral source with a 7 mm-diameter sealing o-ring (see the schematic diagram in ref. 11). The optical system of the instrument consists of an $f = 0.75$ m Paschen–Runge vacuum polychromator with 34 fixed channels with photomultipliers, creating a spectral resolution of ≈ 25 pm. A constant discharge voltage/discharge current of 850 V/15 mA in argon was used in the measurements. Sputter rate-corrected calibration was established on this instrument, based on certified reference materials of titanium with impurities and various titanium alloys, the closest of which to the Ti–6Al–4V composition were the materials 101X Ti3 A (MBH Analytical Ltd, UK), IARM 178C (ARMI International, USA) and RTi 13-10 (SUS GmbH, Germany). A two-point calibration was set up for hydrogen, based on pure titanium and a TiH$_2$ layer on Ti.[12] Calibration for oxygen was made using several low-oxygen titanium samples, and, as a high point, an iron oxide layer on steel (calamine).[14] Emission yields were calculated by linear regression, as the slopes of the intensity *vs.* (c.q) plots, while subtracting the spectral background of the respective line.[8]

To be able to correct for hydrogen effects in some elements, GDOES spectra of pure elements were collected in pure argon and the (Ar + 0.25% H$_2$) mixture, at the same discharge current and voltage, using the GDS500A spectrometer (LECO Corp., USA). This is an instrument with CCD detectors and a spectral

Table 1 Emission lines used in the GDOES analysis and parameters relevant to 'hydrogen corrections' in the depth profile quantification

	λ/nm	$\xi_{Ar–ArH}$	α_E
Ti 399	399.864	0.457	−0.350
H 121	121.467		
C 165	165.701		
N 149	149.262		
O 130	130.217		
Al 396	396.152	0.552	−0.289
V 411	411.178	0.411	−0.380

resolution of ≈ 65 pm. Emission lines used for the elements analyzed are listed in Table 1, together with intensity ratios of these lines in pure Ar and the Ar–H$_2$ mixture, denoted as $\xi_{Ar–ArH}$, and the corresponding hydrogen-correction factors (see eqn (2) and the description of the correction procedure under Results).

Independent bulk analysis of hydrogen in the samples under study was performed by inert gas fusion (IGF)[7] using the G8 Galileo ONH analyzer, Bruker AXS GmbH, Germany. Depth distributions of heavy elements Ti, Al, and V after the sample was ground away (see below) were also established by energy-dispersive X-ray spectroscopy (EDX) using the instrument EDAX Octane Super 60 mm^2, while a wedge-shaped groove was first created on the sample surface by a xenon focused ion beam (FIB) using scanning electron microscope (SEM) Tescan FERA 3, so that the resulting lateral dimension corresponding to the depth beneath the surface is over 200 μm. The microstructure of the hydrogenated TiAl6V4 material under study was established by electron backscatter diffraction (EBSD) using an FEI 3D Quanta 3D field-emission-gun DualBeam scanning electron microscope.

3. Results

GDOES analyses of unknown† samples were performed in the depth-resolved mode: after the discharge ignition, emission intensities of individual lines were collected as a function of time, and the resulting set of intensity–time profiles was subsequently quantified using the standard quantification procedure, as described in ref. 8. On the original sample surface, an oxide layer was found (see the profile in Fig. 1) at depths down to $d \approx 5$ μm. No correction for hydrogen effects was applied, as hydrogen virtually does not enter the oxide. Therefore, individual element profiles within the oxide layer are deemed quantitative, unlike deeper in the sample where the intensities are affected by hydrogen. It is not the purpose of this work to comment on the rather complex depth distributions of individual elements within the oxide layer; the goal here is to analyze the hydrogenated material.

As glow discharge sputtering proceeds deeper into the sample, a peculiar behavior is observed: the hydrogen-rich zone beneath the oxide, the beginning of which is apparent in Fig. 1 at depths below ≈ 5 μm, extends down to ≈ 30 μm and is followed by a zone virtually free of hydrogen. To obtain information from greater depths than those accessible by glow discharge sputtering, the samples were ground, step-by-step,
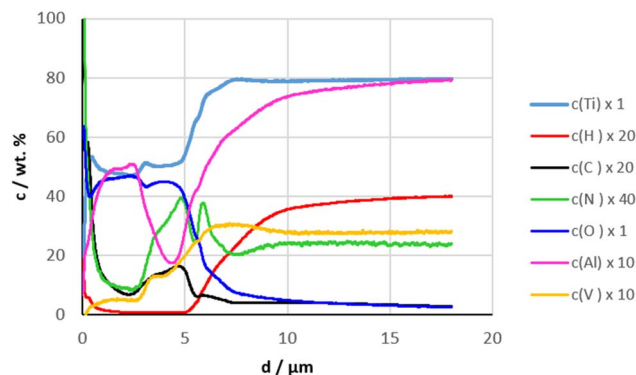
This journal is © The Royal Society of Chemistry 2024

J. Anal. At. Spectrom., 2024, **39**, 996–1003 | **997**

Fig. 1 GDOES depth profile of the topmost region of hydrogenated Ti–6Al–4V with an oxide layer. Abscissa: the depth below the surface, ordinate: concentrations in weight percent. Scaling factors listed in the legend were applied to individual element curves, to match well the coordinate scaling. Below ≈ 5 μm the profiles are qualitative-only (no hydrogen-corrections applied).

down to the depths of several hundred μm and analyzed by GDOES. The observed depth distributions after each grinding step were very similar: on top, there is always a hydrogen-rich zone, followed by a material virtually free of hydrogen, see Fig. 2, after ≈ 700 s of sputtering. This is surprising, as the

Fig. 2 GDOES composition *vs.* sputtering time profile of hydrogenated Ti–6Al–4V after $a \approx 0.5$ mm thick layer was ground away. (Top) The profile quantified without correction for hydrogen effects, (bottom) the same profile with H-corrections applied.

average hydrogen content established by IGF is $\approx 0.6\%$ throughout the sample and no signs of any discontinuities in hydrogen distribution were found by sectioning the sample and subsequent IGF analyses of individual sections. Also, the emission intensity of the H 121 line in the hydrogen-rich zone is much higher than what would correspond to the actual hydrogen concentration established by IGF. Hydrogen concentrations, as resulting from GDOES analyses based on the calibration by TiH_2, are therefore unrealistically high (see the plots in Fig. 1 and 2).

The concern in this work was about the composition rather than accurate depths, hence, the profiles shown in Fig. 2 are displayed as composition *versus* time of sputtering instead of composition *versus* depth, so that H-effects on excitation processes (emission yields) of the other elements can be separated from intensity variations caused by a drop of the sputtering rate, also related to the presence of hydrogen.[11] In this way, the interpretation of the resulting GDOES depth profiles can be simplified. Linear hydrogen corrections of the type

$$R_E \rightarrow R_E' = R_E(1 + \alpha_E I_H) \tag{2}$$

where I_H is the intensity of the hydrogen line, were applied to the emission yields of major matrix elements (Ti, Al, V), as described in ref. 11. The α_E coefficients, listed in Table 1, were established based on the respective ξ_{Ar-ArH} intensity ratios in pure Ar and the (Ar + 0.25% H_2) mixture, also listed in Table 1, by the following relation:

$$\alpha_E = \eta(\xi_{Ar-ArH}(E) - 1) \tag{3}$$

where η is an instrument-dependent factor, common for all the elements E to be corrected and reflecting the gain (detector setting) of the hydrogen channel. By comparison of the top and the bottom plots in Fig. 2, it is apparent that the H-corrections mentioned above largely remove the observed differences in the signal response of these elements between the hydrogen-rich and hydrogen-free zones. This means that, in fact, only very small changes of the concentrations of matrix elements occur in the subsurface region, compared to the bulk material. This is in conformance with the results obtained by EDX microanalysis: virtually no variations of the matrix composition over the depth corresponding to the depth profiles in Fig. 2.

The results described above suggest that, most likely, hydrogen from the bulk material in which it was uniformly distributed, diffuses during the GDOES analysis towards the analyzed surface and enters the discharge at a higher rate than without diffusion, leaving behind a zone depleted of hydrogen. There is a brief discussion of the mechanisms that are likely involved in the following section.

4. Discussion

The cathode material (the sample) is subjected to thermal heating from the glow discharge plasma, which boosts the diffusivity of hydrogen in the material. To assess the thereby induced changes of hydrogen distribution, heat conduction and the kinetics of the thereby caused hydrogen redistribution
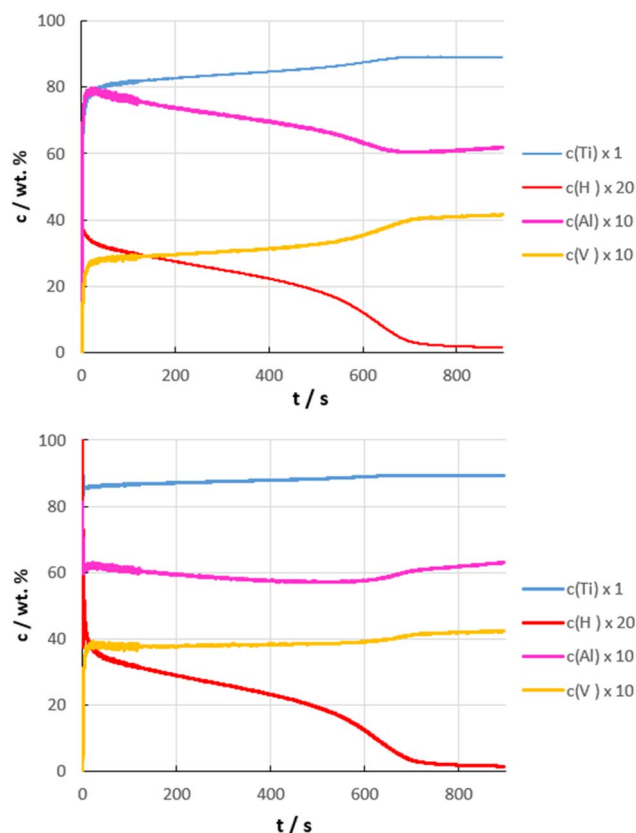
processes must be considered. The structure of the material plays a major role in this, especially in 3D-printed materials (see *e.g.* ref. 5, 6, 15 and 16).

Temperature distribution T within the sample, beneath the analyzed surface, is a function of spatial coordinates and time, and is described by the heat conduction equation,[17]

$$\text{div}(k\nabla T) = c\rho \frac{\partial T}{\partial t} \tag{4}$$

where t is time, k is the thermal conductivity coefficient, c is the heat capacity and ρ is the density of the sample material. To assess the temperature distribution, the geometry of the sample and the way it cools need to be considered. For relatively thin samples, *i.e.*, sheets with a thickness much smaller than the dimensions of the analyzed spot, cooled from behind, a one-dimensional approximation can be used, in which, after the steady state of heat transfer has been reached, eqn (4) becomes

$$\frac{\mathrm{d}^2 T}{\mathrm{d}x^2} = 0 \tag{5}$$

provided that the thermal conductivity coefficient k is constant. The x-axis is perpendicular to the sputtered surface and the variable x denotes the depth within the sample. Temperature $T(x)$ then decreases linearly with x. Heat flux across the sample is then constant (does not depend on x) and is approximately equal to the power dissipated in the discharge. If the outer side of the sample is held at a temperature not much higher than the room temperature, T_{room}, the temperature difference between the analyzed and the outer surface of the sheet will be

$$T_\mathrm{a} - T_{\text{room}} = \frac{\Phi \cdot L}{k} \approx \frac{L}{k} \frac{Ui}{\pi R^2} \tag{6}$$

where Φ is the heat flux density, L is the thickness of the sample (sheet/slab), U and i are the voltage and the current of the discharge, respectively, and R is the radius of the analyzed spot. Another case, also relevant to GDOES, in which eqn (4) can be easily solved, is a bulk sample, also cooled from behind, the dimensions of which are much bigger than the size of the analyzed spot. Such a sample can be approximately represented by a hemisphere, the flat side of which is attached to the discharge source. Instead of x, radial coordinate r can be introduced, with zero in the middle of the analyzed area, expressing the distance from the analyzed spot in any direction within the sample, not only in the direction perpendicular to the analyzed surface. For $r \gg R$ and the sample being uniformly cooled at the curved part of the hemisphere, temperature distribution within the sample will be (almost) radially symmetrical relative to the center located at $r = 0$. For such case, eqn (4) will turn into

$$\text{div}(k\nabla T) = k \frac{1}{r^2} \frac{\partial}{\partial r}\left(r^2 \frac{\partial T}{\partial r}\right) = c\rho \frac{\partial T}{\partial t} \tag{7}$$

and, for the steady state, it will become an ordinary differential equation with a single variable, r:

$$\frac{\mathrm{d}^2 T}{\mathrm{d}r^2} + \frac{2}{r} \frac{\mathrm{d}T}{\mathrm{d}r} = 0 \tag{8}$$

This equation can be solved analytically and its solution is

$$T(r) = a + \frac{b}{r} \tag{9}$$

where a and b are constants that can be established from boundary conditions, *i.e.*, the entering heat flux ($U \cdot i$), the size of the sample‡ and the temperature at its cooled surface:

$$a = T_{\text{room}}, \quad b = \frac{U \cdot i}{2\pi k} \tag{10}$$

Temperature at the analyzed spot of such a bulk sample can then be roughly estimated by considering unidirectional heat flux perpendicular to the analyzed surface for $r \le R$, followed by radially symmetrical propagation of the heat, eqn (7), for $r > R$ (see Fig. 3).

Heat propagation for $r \le R$ can be treated based on eqn (6), separately for each segment (annulus) between (r, $r + \mathrm{d}r$). The solution with a constant temperature $T(R)$ at the hemisphere $r = R$, independent of the azimuthal angle, assumes a non-uniform temperature distribution over the analyzed spot, reaching a maximum at the center. Its average value can be estimated by replacing the hemisphere $r = R$ by a cylinder, with the base at the analyzed spot and an effective thickness, R_{eff}, equal to the averaged distance between the base and the surface of the hemisphere $r = R$. Simple geometrical considerations lead to the value $R_{\text{eff}} = \frac{2}{3}R$. According to eqn (6) and coming back to the model (notation) depicted in Fig. 3, the average surface temperature at the analyzed spot will be

$$T_\mathrm{a} \approx T(R) + \frac{2}{3} R \frac{1}{k} \frac{U \cdot i}{\pi R^2} = T(R) + \frac{2}{3} \frac{U \cdot i}{k \pi R} \tag{11}$$

where $T(R)$ is the temperature at the hemisphere $r = R$. Suppose the characteristic size of the bulk sample (the radius of the model hemisphere) is R_s. The temperature difference between $r = R$ and the outer surface of the sample, held at room temperature, can be established from eqn (9) and (10):

$$T(R) - T_{\text{room}} = \int_{R_\mathrm{s}}^{R} \mathrm{d}T = -\frac{U \cdot i}{2\pi k} \int_{R_\mathrm{s}}^{R} \frac{\mathrm{d}r}{r^2} = \frac{U \cdot i}{2\pi k}\left(\frac{1}{R} - \frac{1}{R_\mathrm{s}}\right) \tag{12}$$
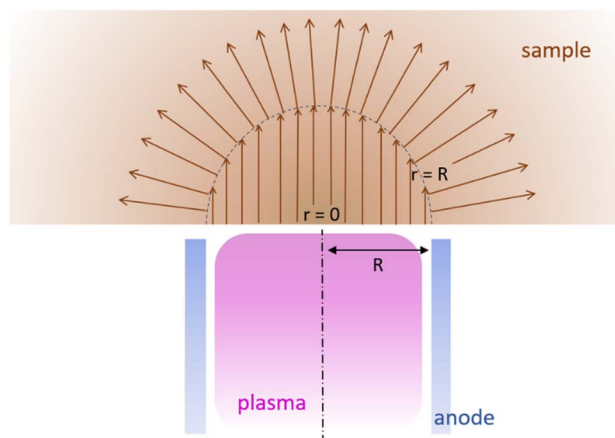
Fig. 3 Model of heat propagation in a bulk sample in the GDOES analysis.

This journal is © The Royal Society of Chemistry 2024

J. Anal. At. Spectrom., 2024, **39**, 996–1003 | **999**

This, combined with eqn (11), gives

$$T_a - T_{room} \approx \frac{U \cdot i}{2\pi k} \left[\frac{1}{R} \left(1 + \frac{4}{3} \right) - \frac{1}{R_s} \right] \quad (13)$$

and, for a large sample ($R_s \to \infty$),

$$T_a - T_{room} \approx \frac{7}{6\pi} \frac{U \cdot i}{kR} \quad (14)$$

If, instead of the 'average' temperature T_a, the temperature in the center of the analysed spot, T_m, is of interest, the factor $\frac{2}{3}$ in eqn (11) needs to be replaced by one. Eqn (13) then becomes

$$T_m - T_{room} \approx \frac{Ui}{2\pi k} \left[\frac{3}{R} - \frac{1}{R_s} \right] \quad (15)$$

and, for a large sample ($R_s \to \infty$),

$$T_m - T_{room} \approx \frac{3}{2\pi} \frac{U \cdot i}{kR} \quad (16)$$

By comparing this with eqn (6) it is possible to assess how the surface temperature of a thin sample will differ from the surface temperature in the center of the analyzed spot of a bulk sample at the same discharge conditions.

The samples described here were 3 mm thick slabs, ≈ 7.5 mm wide and 15 mm long, and the radius of the analyzed spot was $R \approx 1.2$ mm. Such sample is neither "thin", to conform with the presumptions of eqn (6), nor does it resemble a hemisphere. However, at such geometry, heat flux occurs at a non-negligible rate also in directions not perpendicular to the analyzed surface. Hence, an appropriate formula to estimate the surface temperature in the center of the analyzed spot is eqn (15), with $R = 1.2$ mm and $R_s = 3$ mm. The heat flux ($U \cdot i$), for a discharge running at 850 V and 15 mA, is 12.75 W. The thermal conductivity coefficient at room temperature of Ti6Al4V is $k \approx 7$ W m^{-1} K^{-1} and linearly increases with temperature, to ≈ 20 W m^{-1} K^{-1} at 1100 K (827 °C).[18] With $k = 7$ W m^{-1} K^{-1}, eqn (15) gives $T_m = 648$ °C. This means that the temperature dependence of k can in no way be neglected and the considerations presented above should be refined by solving eqn (4) and (7) with a temperature-dependent k instead of k being a constant. Or, for simplicity, eqn (15) can still be used for a raw estimate, however, with a higher thermal conductivity coefficient than the mentioned value of 7 W m^{-1} K^{-1}. For example, for $k = 12.74$ W m^{-1} K^{-1}, eqn (15) gives $T_m = 365$ °C. At this temperature, the function $k = k(T)$ mentioned above gives exactly the same value of k (a self-consistent solution). The thermal conductivity coefficient deeper in the sample, for $r > R$, will be lower than the suggested value of 12.74 W m^{-1} K^{-1}, and close to the surface it will be higher. For a more accurate estimate of T_m, the heat transfer equation would have to be solved with temperature-dependent thermal conductivity. The estimated temperature distribution within the sample, on the axis perpendicular to the analyzed area and going through its center, calculated for $k = 12.74$ W m^{-1} K^{-1}, is given in Fig. 4. The depth of the erosion crater corresponding to 600 s of sputtering (Fig. 2), *i.e.*, a typical depth l at which the effects under study
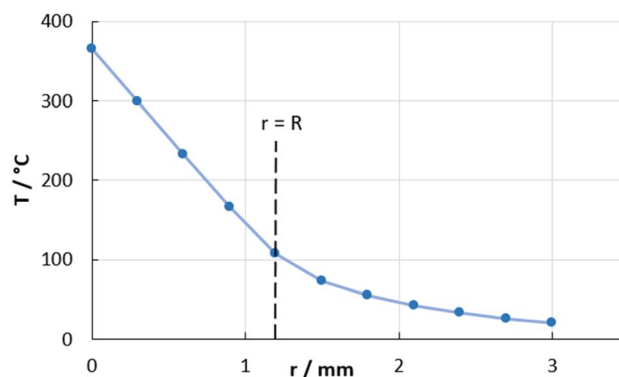

Fig. 4 The estimated temperature distribution along the line perpendicular to the analyzed area and crossing its center, for $k = 12.74$ W m^{-1} K^{-1}, according to the model described in the text.

occur, is only ≈ 30 μm, and temperature at such depths will be very close to the surface temperature of the sample (see Fig. 4). This is why the surface temperature is so important in these considerations.

Ti6Al4V is a duplex alloy consisting of two phases: a hexagonal close-packed phase (hcp, α) and a body-centered cubic phase (bcc, β). Hydrogen stabilizes the β phase, lowers the temperature of the α → β transition and changes the α/β ratio in the microstructure in favor of the β phase. At high hydrogen concentrations, precipitation of hydrides may occur. However, in the present study, no hydrides were observed by EBSD in the hydrogenated material and hydrogen is present largely as a solid solution in the β phase. Diffusivity of hydrogen in the β phase is much higher than in α, almost by 3 orders of

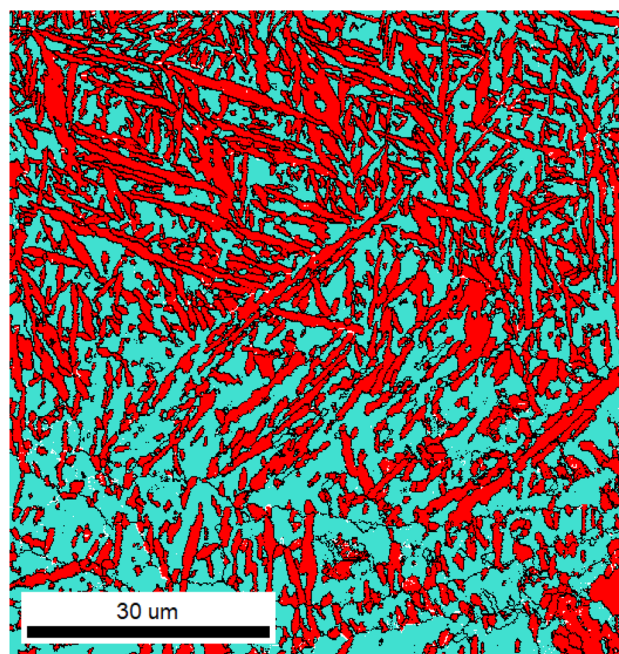**Fig. 5** The structure of the material under study, as revealed by electron backscatter diffraction (EBSD). Red: α phase (hcp), turquoise: β phase (bcc).

1000 | *J. Anal. At. Spectrom.*, 2024, **39**, 996–1003

This journal is © The Royal Society of Chemistry 2024

magnitude at room temperature.[19] The structure of the hydrogenated material, see Fig. 5, is composed of α lamellae in the β matrix, which, together with a dense network of grain boundaries, provides plenty of fast-diffusion pathways for hydrogen, facilitating its high diffusivity mentioned below.

The hydrogenated Ti6Al4V alloy was studied by hydrogen desorption measurements.[5,16] A massive release of hydrogen from the bulk of such material was found to occur between 300 °C and 450 °C, however, the first desorption peak was observed at temperatures as low as ≈200 °C and assigned to hydrogen trapped at dislocations.[5] The second peak, assigned to hydrogen trapped at grain boundaries, occurred at ≈320–340 °C.[5] A further hydrogen evolution at 450–500 °C was assigned to the decomposition of hydrides,[5] which, however, are not present in the material reported here. This means that, in GDOES analysis, an excess flux of hydrogen to the discharge indeed occurs, beyond what would correspond to the flux generated by the sputtering of a material with the originally constant hydrogen concentration. This excess hydrogen comes from the depth of the sample and its transport towards the surface causes gradual depletion of the originally hydrogen-rich subsurface layers. The rate of this transport can be estimated as follows: the diffusion coefficient D of hydrogen in Ti6Al4V exhibits an Arrhenius-type temperature dependence,

$$D = D_0 \exp\left(-\frac{Q}{RT}\right) \qquad (17)$$

with activation energy $Q = 32.80$ kJ mol^{-1},[25] corresponding to the β phase, and a frequency factor D_0 of $\approx 2 \times 10^{-3}$ cm^2 s^{-1}.[24] At the surface temperature of $T = 365$ °C this would yield the hydrogen diffusion coefficient $D = 4.1 \times 10^{-6}$ cm^2 s^{-1}. It drops with temperature, and, therefore, also with the position within the sample. Besides that, temperature at a given position is changing with time before the steady state is reached. As hydrogen leaves the sample, a concentration gradient develops beneath the surface, and this gradient will control the diffusion flux Φ_H of hydrogen:

$$\Phi_H(\boldsymbol{r}, t) = D(\boldsymbol{r}, t)\nabla c_H(\boldsymbol{r}, t) \qquad (18)$$

where $\boldsymbol{r}$ is location and t is time. Hydrogen concentration in the sample will then follow the diffusion equation

$$\frac{\partial c_H(\boldsymbol{r},\ t)}{\partial t} = \nabla\Phi_H(\boldsymbol{r},\ t) = \nabla[D(\boldsymbol{r},\ t)\ \nabla c_H(\boldsymbol{r},\ t)] \qquad (19)$$

The emission intensity $I_H(t)$ of the hydrogen line will no longer reflect the original depth distribution of hydrogen within the sample, $c_H(x, t = 0)$, where x is the same coordinate as that used in the one-dimensional notation in eqn (5), but the instantaneous surface concentration of hydrogen at the time of sputtering, $c_H(x = 0, t)$, where $c_H(x = 0, t)$ is the solution of eqn (19), plus the additional flux of hydrogen due to diffusion.

As the hydrogen-depleted zone grows thicker and becomes exposed to the discharge, it ultimately becomes a barrier for further hydrogen transport from the depth and the hydrogen emission intensity will drop, in conformance with the observation. Moreover, the excess flux of hydrogen in the early stages of the analysis impairs hydrogen quantification in GDOES depth profiles if this effect is not accounted for in calibration, also in conformity with the observations. The depth at which an almost complete depletion by hydrogen occurs is $l \approx 30$ μm, after ≈600 s of sputtering (see Fig. 2). Considering the value of D mentioned above, the characteristic diffusion velocity D/l would be ≈13 μm s^{-1}, which is more than two orders of magnitude higher than the sputtering rate of the sample§, $\xi \approx 30$ μm/600 s = 0.05 μm s^{-1}. This is why a virtually hydrogen-free zone develops below the sputtered surface.

5. Conclusions

Glow discharge optical emission spectroscopy is a viable option for depth-resolved analysis of hydrogenated materials; however, quantitative analysis and the subsequent interpretation of the resulting profiles may not be as straightforward as in other applications of GDOES. The so-called 'hydrogen effects' target some major excitation processes in the glow discharge such as, e.g., charge transfer from Ar$^+$ ions to the analyte atoms.[10] This directly affects populations of certain excited levels of the elements present and via cascade excitation the whole emission spectrum of an element. This makes the resulting picture rather complex and empirically established corrections are needed to achieve analytically meaningful results.[11,20]

Besides that, the resulting hydrogen depth profiles may also be distorted by the redistribution of hydrogen beneath the analyzed surface, due to the elevated temperature below the analyzed spot. It was shown that such transport of hydrogen occurs in the analysis of hydrogenated 3D-printed Ti6Al4V. Hydrogen from deeper-lying layers of the sample diffuses towards the surface and causes an excess flow of hydrogen to the plasma, beyond what would correspond to the sputtering of the sample material with a constant bulk concentration of hydrogen. Not only does this enhance hydrogen emission intensities in the beginning of the analysis, but also a hydrogen-depleted zone gradually develops below the layer being sputtered, hydrogen transport through this zone is hindered, and, after some time of sputtering, hydrogen emission intensities drop. These variations of the hydrogen signal in GDOES analysis of such materials should not be misinterpreted as an originally uneven hydrogen distribution (prior to the analysis). If hydrogen is present only in the top-most layer of the sample and the depth profile extends deeper into the material, the total amount of hydrogen can still be established by integration: all the hydrogen present ultimately enters the plasma and the diffusion within the sample will only change the depth scale, however, the integral of the hydrogen depth profile across the whole analysed depth will remain virtually unaffected.[21]

To suppress hydrogen transport in the sample during analysis, a more efficient sample cooling would be necessary, down to cryogenic temperatures. Such cooling should be turned on only after the sample is placed onto the Grimm lamp and the discharge region pumped down, to avoid the condensation of atmospheric moisture on the surface to be analyzed. Also, the sealing of the discharge source against the atmosphere should

This journal is © The Royal Society of Chemistry 2024

J. Anal. At. Spectrom., 2024, **39**, 996–1003 | **1001**

be taken care of, as the common fluorocarbon (Viton) o-rings get stiff below ≈ -26 °C.[22] Another possibility would be to reduce the power dissipated in the sample by working with pulsed discharge with a small duty cycle instead of the constant dc mode of operation. A drawback of this method is a reduced sputtering rate, unwelcome when deep depth profiles are analyzed.

The concepts and considerations presented here are applicable also in GDOES analysis of other hydrogen-containing materials such as *e.g.* electrodeposited metallic coatings or coatings prepared by chemical vapor deposition (CVD) with hydrogen-containing precursors such as CH_4, SiH_3, PH_3, B_2H_6, *etc.* The procedure to estimate the surface temperature of a sample in GDOES analysis, as described in Section 4, may also be useful when analysing materials with a poor thermal conductance or various thermally labile substances or layers. It is worth mentioning that cathode heating is an issue also in glow discharge mass spectrometry (GDMS).[23]

Conflicts of interest

There are no conflicts to declare.

Acknowledgements

Notes and references

† This adjective is used here to distinguish the samples to be analysed (= "unknown") from calibration measurements, in which "known" reference materials are measured, to collect calibration data.

‡ Sample radius, R_0, cancels itself in expressing the constant b and does not figure in the final formula.

§ Unlike the quantity q_M from eqn (1), *i.e.*, sputtered mass per unit time, ξ is the sputtered depth per unit time.

1 B. Vrancken, L. Thijs, J. P. Kruth and J. Van Humbeeck, Heat treatment of Ti6Al4V produced by Selective Laser Melting: Microstructure and mechanical properties, *J. Alloys Compd.*, 2012, **541**, 177.

2 L. E. Murr, S. A. Quinones, S. M. Gaytan, M. I. Lopez, A. Rodela, E. Y. Martinez, D. H. Hernandez, E. Martinez, F. Medina and R. B. Wicker, Microstructure and mechanical behavior of Ti–6Al–4V produced by rapid-layer manufacturing, for biomedical applications, *J. Mech. Behav. Biomed. Mater.*, 2009, **2**, 20–32.

3 O. N. Senkov and F. H. Froes, Thermohydrogen processing of titanium alloys, *Int. J. Hydrogen Energy*, 1999, **24**, 565–576.

4 M. Losertová, M. Hartmann, I. Schindler and J. Drápala, Hydrogen treatment of titanium based alloys, *IOP Conf. Ser.: Mater. Sci. Eng.*, 2017, **266**, 012007.

5 P. Metalnikov, D. Eliezer and G. Ben-Hamu, Hydrogen trapping in additive manufactured Ti–6Al–4V alloy, *Mater. Sci. Eng., A*, 2021, **811**, 141050.

6 Z. Kacenka, M. Roudnicka, O. Ekrt and D. Vojtech, High susceptibility of 3D-printed Ti-6Al-4V alloy to hydrogen trapping and embrittlement, *Mater. Lett.*, 2021, **301**, 130334.

7 Z. Weiss, Analysis of Hydrogen in Inorganic Materials and Coatings: A Critical Review, *Hydrogen*, 2021, **2**, 225–245.

8 Z. Weiss, Calibration methods in glow discharge optical emission spectroscopy: A tutorial review, *J. Anal. At. Spectrom.*, 2015, **30**, 1038–1049.

9 A. Bengtson and S. Hänström, The influence of hydrogen on emission intensities in GD-OES, consequences for quantitative depth profile analysis, *Proceedings of the 5th International Conference on Progress in Analytical Chemistry in the Steel and Metals (CETAS)*, Luxembourg, 1998, pp. 47–54.

10 P. Šmíd, E. B. M. Steers, Z. Weiss, J. C. Pickering and V. Hoffmann, The effect of hydrogen and nitrogen on emission spectra of iron and titanium atomic lines in analytical glow discharges, *J. Anal. At. Spectrom.*, 2008, **23**, 1223–1233.

11 Z. Weiss and P. Vlcak, Analysis of shallow depth profiles of titanium nitride and N-implanted titanium by GD-OES: The 'hydrogen effect' after the discharge startup and a correction thereof, *J. Anal. At. Spectrom.*, 2017, **32**, 2476–2484.

12 V.-D. Hodoroaba, D. Klemm, U. Reinholz, E. Strub, J. Röhrich, W. Bohne, V. Hoffmann and K. Wetzig, Potential candidates of certified reference material for determination of hydrogen concentration with glow discharge optical emission spectrometry (GD-OES)—A feasibility study, *J. Anal. At. Spectrom.*, 2008, **23**, 460–462.

13 V. Hoffmann, M. Uhlemann, S. Richter and J. Pfeifer, Calibration capacity of hot-pressed hydrogen standards for glow discharge optical emission and mass spectrometry, *Spectrochim. Acta, Part B*, 2021, **176**, 106039.

14 V. Hoffmann, B. Gebel, R. Heller and T. Gemming, Investigation of matrix independent calibration of oxygen in glow discharge optical emission spectrometry, *J. Anal. At. Spectrom.*, 2022, **37**, 1223–1228.

15 S. Bai, L. Liu, C. Liu and C. Xie, Phase-Field Insights into Hydrogen Trapping by Secondary Phases in Alloys, *Materials*, 2023, **16**, 3189.

16 P. Metalnikov, A. A. Kaya, G. Ben-Hamu and D. Eliezer, Effect of different hydrogen fugacities on the microstructure of additively manufactured Ti-6Al-4V, *Mater. Charact.*, 2023, **205**, 113285.

17 H. S. Carslaw and J. C. Jaeger, *Conduction of Heat in Solids*, The Clarendon Press, Oxford Science Publications, New York, 2nd edn, 1988, ISBN 978-0-19-853368-9.

18 K. Li, Z. Zhao, H. Zhou, H. Zhou and J. Jin, Numerical analyses of molten pool evolution in laser polishing Ti6Al4V, *J. Manuf. Process.*, 2020, **58**, 574–584.

19 A. Díaz, I. I. Cuesta and J. M. Alegre, Modelling hydrogenation during cold dwell fatigue of additively manufactured titanium alloys, *Procedia Struct. Integr.*, 2021, **34**, 229–234.

20 Z. Weiss, Propagation of uncertainty in multi-matrix analysis by GD-OES, *J. Anal. At. Spectrom.*, 2001, **16**, 1275–1282.

21 J.-C. Wu and T.-I. Wu, Influences of the cyclic electrolytic hydrogenation and subsequent solution treatment on the hydrogen absorption and evolution of β-solution treatment on the hydrogen absorption and evolution of β-solution

treated Ti-6Al-4V, *Int. J. Hydrogen Energy*, 2008, **33**, 5651–5660.

22 **https://www.mtm-inc.com/how-to-select-o-ring-materials-for-vacuum-applications.html**, 2023, November 23.

23 M. Kasik, C. Michellon and L. C. Pitchford, Effects of cathode heating in a GDMS system, *J. Anal. At. Spectrom.*, 2002, **17**, 1398–1399.

24 H.-J. Christ, M. Decker and S. Zeitler, Hydrogen Diffusion Coefficients in the Titanium Alloys IMI 834, Ti 10-2-3, Ti 21 S, and Alloy C, *Metall. Mater. Trans. A*, 2000, **31**, 1507–1517.

25 C. Yexin, Kinetics of Hydrogen Diffusion in Ti-6Al-4V Alloy, *Rare Met. Mater. Eng.*, 2015, **44**, 553–556s.

This journal is © The Royal Society of Chemistry 2024

J. Anal. At. Spectrom., 2024, **39**, 996–1003 | **1003**